polymer

ELSEVIER

Structural heterogeneities and mechanical properties of vinyl/dimethacrylate networks synthesized by thermal free radical polymerisation

Laurent Rey[a], Jannick Duchet[a,*], Jocelyne Galy[a], Henry Sautereau[a], Dominique Vouagner[b], Lionel Carrion[b]

[a]*Laboratoire des Matériaux Macromoléculaires UMR CNRS 5627, Institut National des Sciences Appliquées, Bât. Jules Verne, 20, avenue Albert Einstein, 69621 Villeurbanne Cedex, France*
[b]*Laboratoire de Sciences et Ingénierie des Surfaces (EA 1877), Université Claude Bernard, Lyon 1, 43 bd du 11 Novembre 1918, 69622 Villeurbanne Cedex, France*

Abstract

Dimethacrylate based networks usually have a poor impact resistance. In this work, we have tried to understand the origin of this brittleness. Two systems based on a same dimethacrylate monomer polymerised with styrene and divinylbenzene comonomers, respectively, have been chosen to correlate structural parameters with mechanical properties. The increase of structural heterogeneity, characterized by the width of relaxation time distribution, was measured as a function of double bonds conversion using dynamic mechanical tests. Atomic force microscopy observations of network structure after laser ablation show that the heterogeneity of networks is spacially organised due to the formation of microgels and their agglomeration. The presence of microgels strongly affects the polymerisation kinetics and controls the mechanical behaviour. Results show that the more densely crosslinked the network, the more heterogeneous is its structure. The impact resistance is shown to be related to the level of networks heterogeneities. © 2002 Elsevier Science Ltd. All rights reserved.

1. Introduction

Free radical polymerisation of multifunctional monomers produces highly crosslinked networks. Dimethacrylate based networks are frequently used in high performance applications such as dental restorative materials, information storage systems, ophthalmic lenses, … Nevertheless, those networks usually have poor mechanical resistance. The aim of this work is to try to understand the origin of this brittleness and the relationship with the physical and chemical structures.

In a previous study, polymerisation kinetics of dimethacrylate-based networks have been investigated [1,2]. Results show that the reaction kinetics and morphology of the reacting system are strongly affected by the cure temperature and the comonomer structure. In the early stage of the reaction, polymerisation passed from chemical control to diffusion control so that the final conversion and the polymerisation rate depend only on the reactive species mobility. The multifunctional monomer limits diffusion, final conversion and polymerisation rate. Finally, one of the most important characteristics of such materials is the spatial heterogeneity of the network due to the formation of microgels, domains of high crosslinking density, dispersed in a pool of unreacted monomers [3]. The final network morphology is the result of microgels agglomeration into clusters and connection with those clusters [3,4]. The presence of microgels strongly affects the polymerisation kinetics, the spatial distribution of crosslink density and the resulting morphology probably controls the mechanical behaviour.

In this work, several networks synthesized from a same dimethacrylate monomer with various comonomers (styrene, divinylbenzene and tri(ethyleneglycol)dimethacrylate) will be studied in order to correlate structural parameters and morphologies with mechanical properties and especially fracture behaviour. Our study will be divided

---

* Corresponding author. Tel.: +33-4-72438548; fax: +33-4-72438527.
E-mail address: jannick.duchet@insa-lyon.fr (J. Duchet).

Table 1
Composition of the different systems (In each case, 0.2 g of AMBN and 0.5 g of 1-dodecanethiol have been added to the formulation, (a) initial amount of total double bonds; (b) calculated; (c) the total double bond conversion has been measured using near infrared spectroscopy after cure at 90 °C [REY1])

Sample name	D121 (g)	ST (g)	DVB (g)	TriEGDMA (g)	[C=C] (mol/g) (a)	Mean functionality (b)	Total double bond conversion (%) (c)
D121	100	/	/	/	3.68×10^{-3}	4	82
D121/ST	80	20	/	/	4.84×10^{-3}	2.87	75
D121/ST/DVB							
1	80	15	5	/	5.05×10^{-3}	3.09	73
2	80	10	10	/	5.26×10^{-3}	3.32	72
3	80	5	15	/	5.46×10^{-3}	3.57	71
D121/DVB	80	/	20	/	5.67×10^{-3}	3.83	69
D121/DVB/TriEGDMA							
1	80	/	12	10	5.41×10^{-3}	3.88	69
2	80	/	8	20	5.18×10^{-3}	3.92	74
3	80	/	4	30	4.97×10^{-3}	3.96	82
D121/TriEGDMA	80	/	/	39	4.75×10^{-3}	4.00	82

into three parts. First, the structural heterogeneity of networks will be quantified using the distribution of relaxation times measured by viscoelastic tests. Laser surface ablation treatment will be used to investigate a spatial organisation of the network heterogeneity. Average residual stresses will also be compared as a function of the comonomer structure. Then, the mechanical behaviour of such networks will be studied using three-point bending tests at various temperatures. Finally the fracture surface will be analysed using atomic force microscopy in order to propose an explanation concerning the origin of the brittleness of networks.

2. Experimental section

2.1. Materials

Networks prepared in this study were based on tetraethoxylated bisphenol A dimethacrylate (D121) from Akzo-Nobel (80% by weight either 50% of double bonds). Three monomers, styrene (ST) and/or divinylbenzene (DVB) and/or Tri(ethyleneglycol)dimethacrylate (Tri-EGDMA) were added in several proportions as reported in Table 1. Two series of networks have been made. The first one is labelled D121/ST/DVB because it is based on 80 wt% of D121 copolymerised with 20 wt% of ST and DVB. The second one is labelled D121/DVB/TriEGDMA and is based on D121 copolymerised with DVB and TriEGDMA. A same amount of chain transfer agent, 1-dodecanethiol was also used (0.5 phr) in all formulations. All systems were thermally initiated by azobismethylbutyronitrile (AMBN) (0.2 phr). Products were used as received; their chemical structures are shown in Table 2.

The mixing was carried out in a glass vessel with a magnetic stirrer at room temperature during twenty minutes to achieve an homogeneous mixture of all components. The blend was flushed with nitrogen under agitation to remove oxygen in order to avoid inhibition, then the reactive liquid was introduced into a mould made of two glass plates separated by a 2 mm silicone gasket. The crosslinking reaction was conducted in an oven for 8 h at 60 °C, then for 2 h at 90 °C and then slowly cooled down to room temperature. Samples were removed from the mould and then post-cured for 2 h at 120 °C. The final double bond conversion was measured by near infra-red spectroscopy [1] and is reported in Table 1.
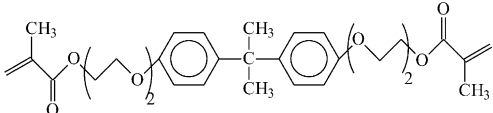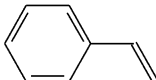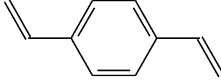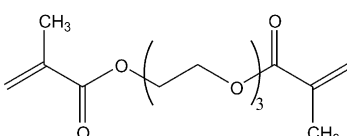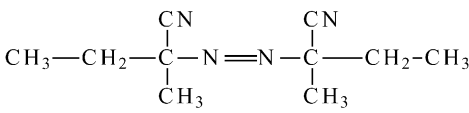
2.2. Characterization

Dynamical mechanical measurements. Dynamical mechanical measurements were performed with a dynamic mechanical analyser (Rheometrics RDAII) in torsion mode with a pulsation of 6.28 rad s^{-1}. Samples were rectangular bars 2 mm thick and overall dimension 35×5 mm^2. The storage shear modulus, G', and tan δ have been recorded as a function of temperature. The rubber modulus, G'_r was measured at 180 °C, well above T_α. T_α is the temperature at the maximum of tan δ peak and h_α is the half-width of tan δ peak.

Atomic force microscopy (AFM). The network surfaces were imaged using an Atomic Force Microscope from Digital Instruments (Multimode Nanoscope 3A) in tapping mode™. Topographic and phase images, corresponding to changes in the amplitude and the phase of the oscillating AFM cantilever probe were recorded to analyse the morphology of sample surfaces after laser ablation treatment or fracture. We have determined the surface roughness, R_A, which is the average roughness and is defined as the arithmetic average of the absolute values of altitude differences (z) compared to a medium plan. This plan is chosen in order to equal the areas in its both side. R_A is calculated using the following expression:

$$R_A = \frac{1}{L} \int_0^L |Z - \bar{Z}| \mathrm{d}x \tag{1}$$

Table 2
Chemical products used in synthesis of materials

Name	Chemical formula
Dimethacrylate of tetraethoxylated bisphenol A (D121®) *Akzo-Nobel*	Stabilized by 100–200 ppm of p-methoxyphenol
Styrene (ST) *Aldrich*	Purity: 99.7%. Stabilized by 10–15 ppm of terbutylcathecol
Divinylbenzene (DVB) *Fluka*	80% mixture of p- and m isomers; 16% of ethylvinylbenzene; 1.5% of diethylbenzene; 0.5% of naphtalene. Stabilized by 900–1090 ppm of terbutylcathecol
TriEthyleneGlycol Dimethacrylate (TriEGDMA) *Aldrich*	Purity: 95%
1, Dodecanethiol *Aldrich*	Purity: 98%
Azobis methyl butyronitrile Vazo 67® (AMBN) *Dupont*	Purity: 98%

Laser ablation treatment. Laser ablation treatment has been used to study the structure of networks. Polymer plates have been prepared in the same manner as previously reported. Nevertheless, a silicone wafer has been introduced in the mould in order to create a flat surface at the nanometric scale. The experiments were carried out at atmospheric pressure and room temperature. A picosecond modelocked Nd^{3+}-YAG laser has been used at a repetition rate of 10 Hz to ablate the polymer surface. The applied wavelength was its fifth harmonic at 213 nm with a pulse duration of 16 ps. The laser pulse energy was measured by using a joulemeter probe (Laser Precision Ref RJ 7620). The laser beam was sent first through a diaphragm and then focalised on the sample using a UV (CaF_2) lens. The role of the diaphragm was to obtain a more homogeneous distribution of the incident energy. In fact, the spatial distribution of the energy in lasers is not uniform but has a gaussian shape. In this case, it is difficult to measure the

beam diameter whose value is necessary to determine the fluence received by the sample. With a diaphragm, the edges of the gaussian curve are eliminated and only the central part of the beam is sent onto the sample. Thus, the laser beam diameter can be assimilated to that of the diaphragm.

The ablation treatment parameters were determined and optimised to obtain a moderate ablation without polymer degradation [5]. The applied laser fluence was set to 7.6×10^{12} W/cm^2 for all experiments. Samples were illuminated during 120 s and the irradiated spot was 700 μm in diameter. In accordance with Feng, the number of pulses (1200) was adjusted to obtain a significant ablation for our experiments [6].

Residual stresses measurements. The stress build-up was measured by beam-bending technique. A 2 mm layer of reactive mixture was applied to an aluminium beam ($50 \times 10 \times 0.23$ mm^3). The deflection at the centre of the beam, *d*, was measured after cure and post-cure. The stress

level was calculated from the measured deflection according to the following expression [7]

$$\sigma = -\frac{E_2 h_2^2}{6 h_1 R} \frac{1}{(\alpha\beta + 1)} \left\{ 1 + \beta(4\alpha - 1) \right.$$
$$\left. + \beta^2 \left[\alpha^2(\beta - 1) + 4\alpha + \frac{(1 - \alpha)^2}{\beta + 1} \right] \right\} \quad (2)$$

where index 1 denotes polymer, 2 denotes substrate; E_i is the modulus of the layer i, h_i the thickness of the layer i, $\alpha = E_2/E_1$, $\beta = h_2/h_1$ and $\beta < 1$, L_2 the span distance, d is the deflection at the centre of the beam and $R = L_2/8d$.

Three-point bending tests. Three-point bending tests were performed on a 2/M MTS testing machine at several temperatures between -70 and $75\,°C$. Samples ($2 \times 50 \times 5\,mm^3$) have been fitted to have a span to thickness ratio of 20. The crosshead speed was fixed to 1 mm/min. The maximum flexural stress, σ_F, was calculated following the relationship

$$\sigma_F = \frac{3FL}{2bh^2} \quad (3)$$

where F is the load, L the span length, b the width and h is the thickness. The flexural strength was defined as the energy required to fracture the testing sample divided by its cross-section.

3. Results and discussion

Styrene, Divinylbenzene and TriEGDMA have been used as comonomer to synthesize networks having varying properties. The study will be mainly focused on two networks labelled D121/ST and D121/DVB. Those systems have been selected because of their very different impact behaviour. D121/ST system is the toughest network ($12.6\,kJ/m^2$) and D121/DVB network is the most brittle one ($3.6\,kJ/m^2$) when tested by Charpy impact tests at room
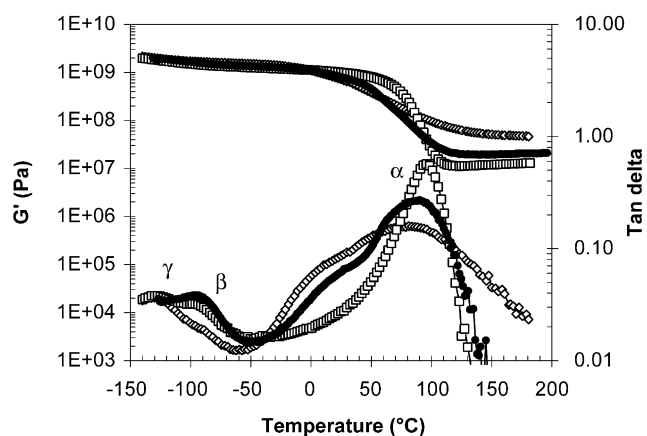

Fig. 1. Evolution of the storage modulus G' and tan δ as a function of temperature (at frequency 1 Hz) for D121 (●), D121/ST (□) and D121/DVB (◇) networks.

temperature. Results concerning the other networks will be used as extensions to improve conclusions found from D121/ST and D121/DVB network investigations.

3.1. Network heterogeneity and morphology

3.1.1. Determination of a structural heterogeneity parameter

Viscoelastic properties of all networks have been characterised in a torsion mode after post-cure. Fig. 1 depicts a typical evolution of the shear modulus, G' and tan δ as a function of the temperature for D121, D121/ST and D121/DVB.

Two secondary relaxations have been detected for all networks. The γ transition around $-130\,°C$ has an activation energy of 20 kJ mol^{-1} and can be attributed to motions of local groups on the main chain such as methyl rotation [8]. A second one, β, near $-100\,°C$ has an activation energy of 34 kJ mol^{-1} and can be attributed to the rotation of 2 or 3 ethoxy groups in the dimethacrylate chain [8,9]. Both have a low intensity, γ is not strongly affected by the choice of the comonomer but β peak decreases for D121/DVB.

Conversely, the structure of the comonomer has a strong influence on the main α transition. For D121/ST network, the main transition begins near 25 °C and the rubbery state is reached at 120 °C. The main transition is very different when DVB is used as comonomer. When the temperature is higher than -25 °C a part of the network is already in a rubbery state and the end of the main transition occurs near 180 °C. The use of DVB increases the width of the α transition: some parts of the network are loosely crosslinked and extend the main transition to lower temperatures (down to -25 °C) and in the same network some parts are very densely crosslinked and enlarge the main transition to higher temperatures (up to 180 °C).

These observations concerning the distribution of relaxation times suggest that the heterogeneity of the D121/DVB network structure is higher than the D121/ST one. The distribution of relaxation times is a direct measurement of the polymer chain mobility in the network. Therefore, a quantification of the distribution of relaxation times provides a good parameter of the degree of heterogeneity of the network structure. The evolution of the modulus during the α relaxation is often used to quantify the distribution of relaxation times using the well-known Kohlrauch–Williams–Watts stretched exponential function [4]

$$E(t) = E_0 \exp[-(t/\tau)^\beta] \quad (4)$$

β takes a value between 0 and 1. β is close to 1 when the distribution of relaxation times is narrow and close to 0 if it increases. In order to measure an accurate value of β, the modulus must be measured over a wide range of relaxation times. The time temperature superposition has been used to
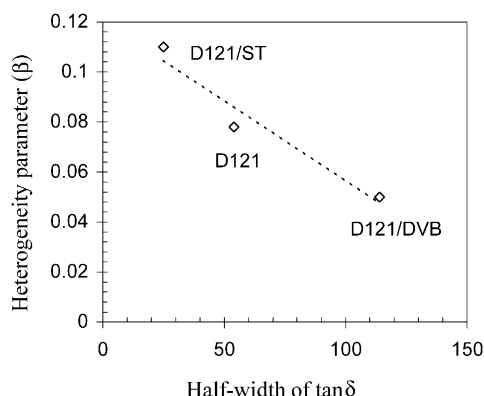
Fig. 2. Evolution of the heterogeneity parameter β as a function of the half-width of tan δ for D121, D121/ST and D121/DVB networks.

produce a master curve from measurements at different temperatures in a large range of frequencies (from 0.16 to 16 Hz). The following approximation has been used to convert data from frequency ν to time regime [10].

$$E(t) \approx E'(\nu = 1/t) \tag{5}$$

The value of β is equal to 0.11 for D121/ST, the most homogeneous network, 0.078 for the D121 network and 0.05 for D121/DVB, the most heterogeneous network. As plotted in Fig. 2, there is a linear relationship between β and the half-width of tan δ. It means that both parameters, β and tan δ half-width, are suitable to characterise the structural heterogeneity of networks studied here. In the following studies, the half-width of tan δ will be used as a structural heterogeneity parameter for facility reasons.

The rubbery modulus can be used to evaluate the average crosslinking density of networks by using the rubber elasticity theory, although this theory cannot be applied in a such complicated system [11]. As a result, we will not give values of molar mass between crosslinks $\bar{M}_c$ but the rubbery modulus value will be taken as an indication of the average crosslinking density.

In Fig. 1, it can be observed that the structure of the comonomer has a large influence on the rubbery modulus. DVB acts as a crosslink agent whereas ST acts as a chain extender. As a consequence, the use of ST instead of DVB decreases the mean functionality of the monomer blend (Table 1) and decreases the average crosslinking density of the network formed.

It is interesting to note that D121/DVB is the most highly crosslinked network (highest rubbery modulus) and has also the most heterogeneous structure (the lowest β). In contrast, the D121/ST is the less crosslinked network and has the most homogeneous structure. The same observation can be done for all networks synthesized from the D121 monomer with various comonomers. As plotted in Fig. 3, the half-width of tan δ, i.e. representative of the structure heterogeneity, increases with the value of the rubbery modulus of the network (representative of the crosslinking density). Those results are in agreement with those of Bowman et al.
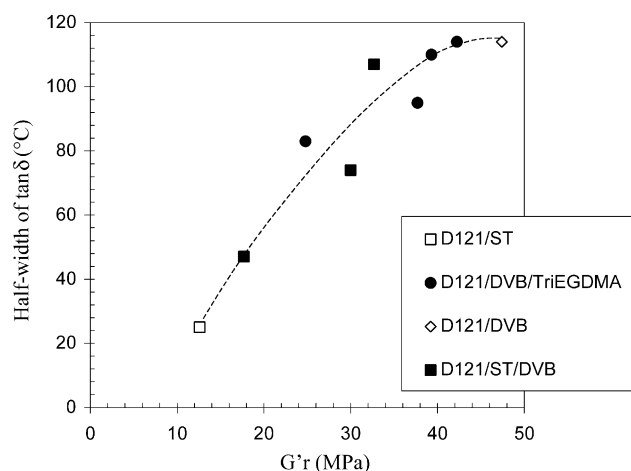

Fig. 3. Evolution of the half-width of tan δ as a function of the rubbery modulus G'_r for several networks synthesized from D121 polymerised with various comonomers.

[10–12], who showed that the structural heterogeneity increases with the amount of crosslinker in similar networks. The use of less flexible (DVB instead of TriEGDMA), or more functional (DVB instead of ST) comonomer leads to an increase in the heterogeneity of the network formed.

As shown in previous studies for the same networks [1, 2], the use of short and highly functional monomers limits the diffusion of reactive species during polymerisation. Some reactive species (radicals or double bonds) linked to the network are not able to diffuse and stay trapped. Very early in the reaction kinetics, termination reactions are diffusion controlled [2]. During polymerisation, the decrease of species reactivity, the steric hindrance of polymer chain and also cyclisation lead to microgel formation and contribute to a very large distribution of relaxation times responsible for the broadening of the main relaxation. Then, in the same material, some parts of the networks are loosely crosslinked and can relax at lower temperatures and some parts of the networks are densely crosslinked and relax at higher temperatures.

3.1.2. Final network microstructure revealed by laser ablation treatment

It is now interesting to know if this large distribution of relaxation times, i.e. crosslinking density, is homogeneously distributed in the network or spatially organised. Preliminary results [1] showed that during isothermal cure at 60 °C, microgel formation occurred for those systems in the early stage of the reaction. The size of the heterogeneities was measured by dynamic light scattering up to the gel time. The size distributions were analysed with bi or tri-modal distributions showing that microgels were first formed followed by the formation of aggregates and large clusters. Bigger clusters were observed with D121/DVB compared with D121/ST. For these not fully cured networks, it has to
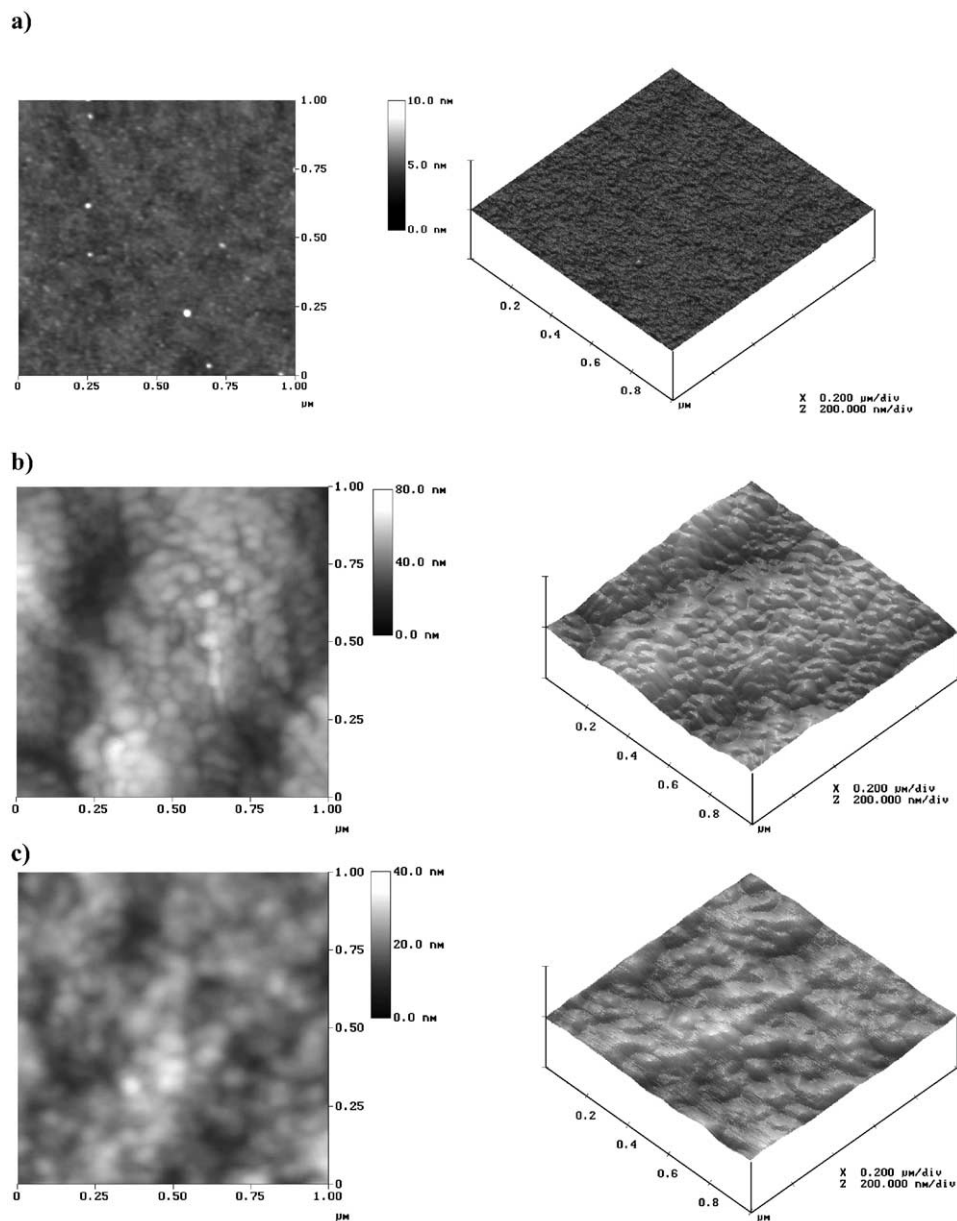
Fig. 4. AFM observations of a reference surface before laser ablation (a), D121/ST (b) and D121/DVB (c) surfaces after laser ablation.

be mentioned that the nodular structure was confirmed by fracture surface analysis by AFM [2].

In order to demonstrate if there is or not a spatial organisation in fully cured networks, laser ablation has been used. Due to the strong absorption of polymers in the UV field and the short duration of the laser pulse (a few 10 ps), laser ablation treatment induces only very localized effects on the surface (between a few tenths of nanometers and a few micrometers) without modifying the bulk material properties. This method, already described by Mortaigne et al. [13], is based on the use of the differences between the thresholds at which ablation of the various constituent phases of the material occurs. Photodissociation can occur because the laser energy used is higher than the bonds

energies relative to the C–C, C–H, O–H and N–H bonds present in most polymers. The ablation rate depends on the chemical composition of the polymer surface. The nature of the physical phenomena taking place during the laser-surface interaction is strongly related to the laser fluence, i.e. the flux of incoming UV photons. In order to obtain the ablation regime, the fluence must exceed a threshold value (ablation threshold) [14]. Below the threshold value, the incident beam induces molecular vibration but no ablation occurs. Nevertheless, the fluence must be optimised to obtain a moderate ablation. In fact, the ablated material is ejected via photo thermal and/or photochemical effects during the ablation regime and because of the low thermal conductivity of polymers, a high fluence value leads to a

surface thermal degradation by polymer vaporisation [15]. Usually, ablation threshold and ablation rate is strongly dependent on the chemical composition of the polymer surface and on the laser wavelength [16]. Mortaigne et al. have developed this technique to analyse the morphology of an unsaturated polyester with a phase rich in crosslinked polyester (microgels) included in a polystyrene matrix. The authors have shown that the ablation threshold of polystyrene was lower than polyester one. Thus, after a laser treatment with a suitable energy intensity, i.e. fluence above the ablation threshold for polystyrene and below the ablation threshold for polyester, Mortaigne et al. observed by scanning electron microscopy nodules attributed to polyester microgels in a polystyrene phase [13]. As a result, a contrast was created by the difference in the ablation rate between the two phases.

The chemical composition of materials studied here is not very different because networks are synthesized from monomers with very similar chemical groups (phenyl groups, C=C and C=O double bonds, C–C single bonds,…). As a consequence, for a same laser treatment, differences in the ablation rate depend on the network structure: in loosely crosslinked part of the network, the ablation of dangling chains will be easier than in highly crosslinked part of the network where the ablation supposes the split of almost all polymer chains. For very similar networks and the same laser treatment, the ablation rate will depend on the local crosslinking density of the network. First, we have determined the ablation threshold to reach the ablation regime without getting polymer degradation. Thus, with the optimised processing parameters (fluence: $7.6 \times 10^{12} \, W \, cm^{-2}$ during 120 s), the laser beam can selectively etch the constituent phase of polymer. As reported in Fig. 4, the laser ablation treatment reveals the morphology of surfaces of D121/ST and D121/DVB fully cured networks. The laser treatment reveals in both cases a nodular structure. On the other side, we have performed a similar experiment on an amorphous PMMA plate and we have observed by AFM an uniform surface without nodule. Nodules diameter observed on the both networks is about 50 nm and can be compared to microgel diameter measured by dynamic light scattering just before gelation in a previous study [2]. Then, the nodular morphology is the result of the growth of the network through the formation of microgels, their agglomeration into clusters and the linking of those clusters. Ziaee et al. [17] have also observed a similar morphology in vinyl-ester networks. This observation is in good agreement with the description of the network build-up proposed by Dusek [3] and adopted by many other research groups.

It is useful to compare the surface roughness of an untreated reference surface (i.e. surface in contact with the silicon wafer) with the surface roughness of laser irradiated surfaces. As shown in Fig. 5, the laser treatment leads to a large increase of the surface roughness compared to the reference surface due to the existence of a nodular
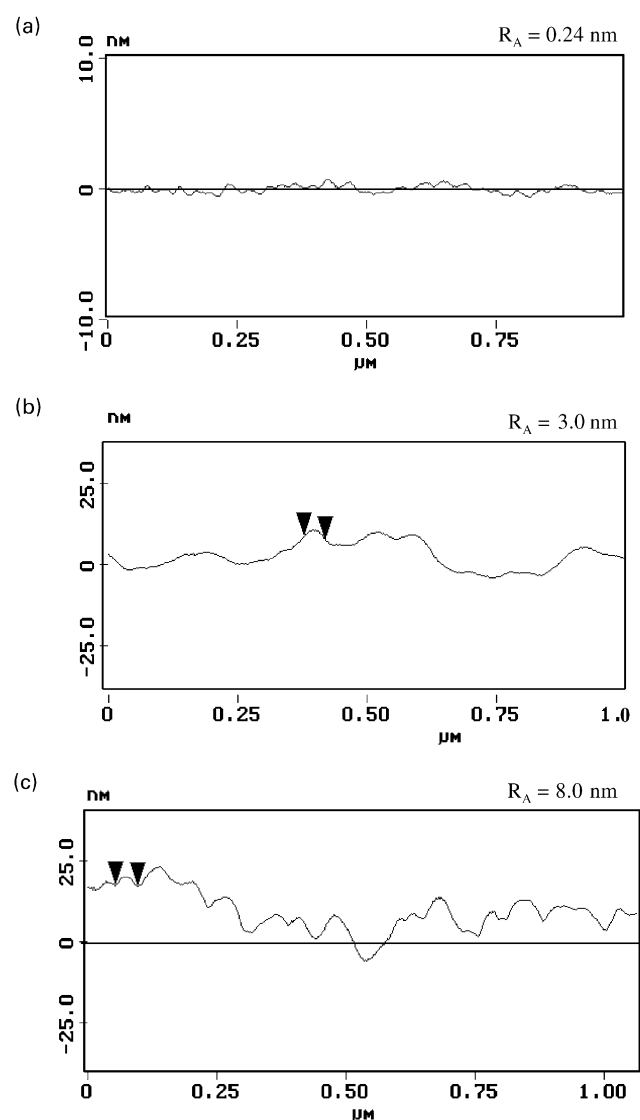

Fig. 5. Comparison of surface profiles and roughness values for a reference surface before ablation (a) and for D121/ST (b) and D121/DVB (c) samples after laser surface treatment.

morphology. Microgel core is more densely crosslinked than the outer shell. Higher values of R_A for D121/DVB surface mean that the difference of crosslinking density between loosely crosslinked parts and highly crosslinked parts is more significant for this network in comparison with D121/ST network.

So from these observations, it can be concluded that the heterogeneity of fully cured networks synthesized from D121 is spatially organised. This organisation is directly linked to microgel formation and agglomeration.

3.2. Mechanical properties

3.2.1. Evaluation of average residual stresses after cure

It is well known that internal stresses occur during the curing of thermosets and that residual stresses may play an
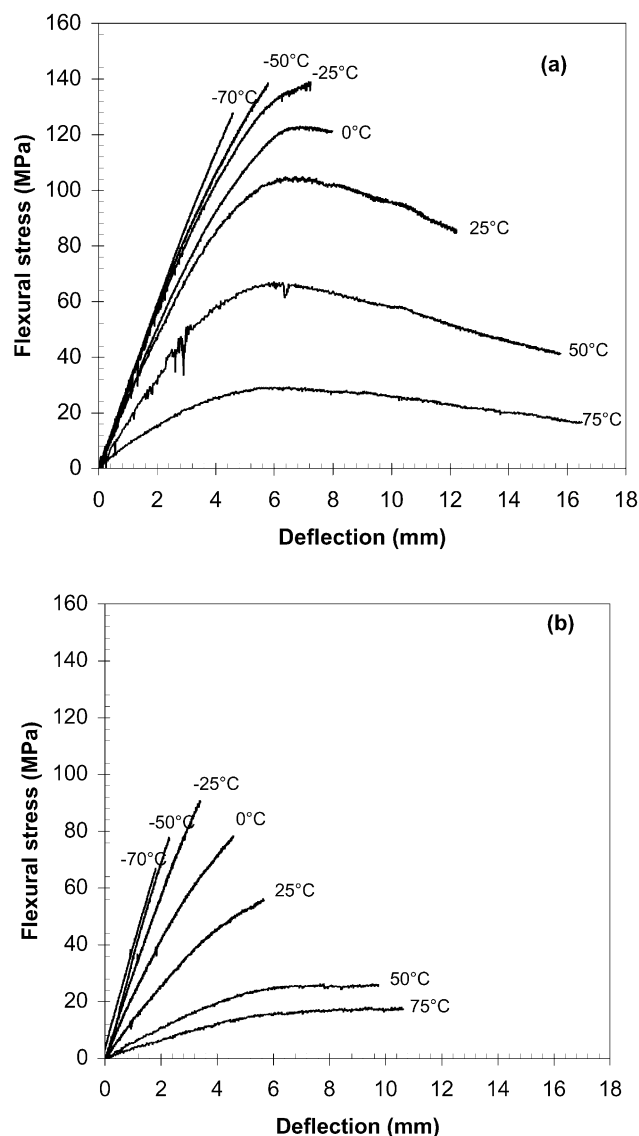
Fig. 6. Typical stress–deflection curves measured in three-point bending tests for D121/ST (a) and D121/DVB (b) networks at different temperatures.

important role in fracture behaviour. Residual stress build-up has been extensively studied in epoxy polymers [18,19] and acrylate networks [20,21]. It has to be noticed that these residual stresses are distributed along the thickness from a compressive stress at the surface to a tensile one at the centre of the specimen. Using the beam-bending technique, we can only have access to the average residual stresses and this method is very useful for comparison with the same geometry samples. As detailed by Lange et al. [21], the origin of these stresses is a mixture of cure and thermal shrinkage. On the one hand, volume shrinkage due to polymerisation reactions creates cure stress. On the other hand, after cure, as soon as the temperature decreases below the T_g of the polymer down to room temperature, cooling stress increases linearly with decreasing temperature depending on the dilatation coefficient of the material. At

Table 3
Comparison of average residual stress level (MPa)

	After cure $T_{max} = 90 °C$	After post-cure $T_{max} = 120 °C$	Evolution (%)
D121/ST	4	8.7	+116
D121/DVB	7.9	11.9	+50

the end of the curing procedure, both stresses after relaxation contribute to the level of residual stresses in the material.

The average residual stresses after cure and post-cure are significantly more important in D121/DVB network compared to D121/ST (Table 3). The stress level is linked with both double bond conversion and crosslinking density. The conversions after post-cure at 120 °C increase slightly: 76% (1.3%) for D121/ST and 72% (4.3%) for D121/DVB networks. The conversions look similar but the crosslink densities for the two networks are very different due to the larger amount of initial double bonds contained in D121/DVB networks (cf. Table 1). It was not possible to achieve a total conversion due to trapped double bonds and by the fact that the post-cure temperature (120 °C, chosen to avoid degradation) was not high enough to give mobility, especially for the D121/DVB networks where the T_α transition spreads up to 180 °C. These results are in good agreement with previous literature [4,21,22] where the residual stress level reached is correlated to the crosslink density (and to the rubbery modulus).

3.2.2. Influence of temperature on the fracture of networks

In order to analyse the consequences of such an heterogeneous structure on the mechanical behaviour, three-point bending tests have been carried out at several temperatures on D121/ST and D121/DVB networks. Typical stress–deflection curves are reported in Fig. 6.

As the temperature increases from −70 up to 75 °C, the mechanical behaviour of the D121/ST network changes from brittle-elastic to plastic with the appearance of a upper yield stress. The flexural modulus decreases with increasing temperature. Higher temperature enhances chain mobility and as a consequence decreases the yield stress. The stress at break decreases and the deflection at break increases. The situation is different for the D121/DVB network. As plotted in Fig. 1, when the temperature is higher than −25 °C, a part of D121/DVB network, probably located around microgels is in a rubbery state. Despite this increasing mobility, no evidence of a plastic propagation (characterised by a upper yield stress) has been measured even at 75 °C where a large part of the network is in a rubbery state. Deflection at break and maximum flexural stress are lower for the D121/DVB network compared to D121/ST and whatever the temperature.

It is useful to compare the evolution of the flexural strength of both networks as a function of temperature
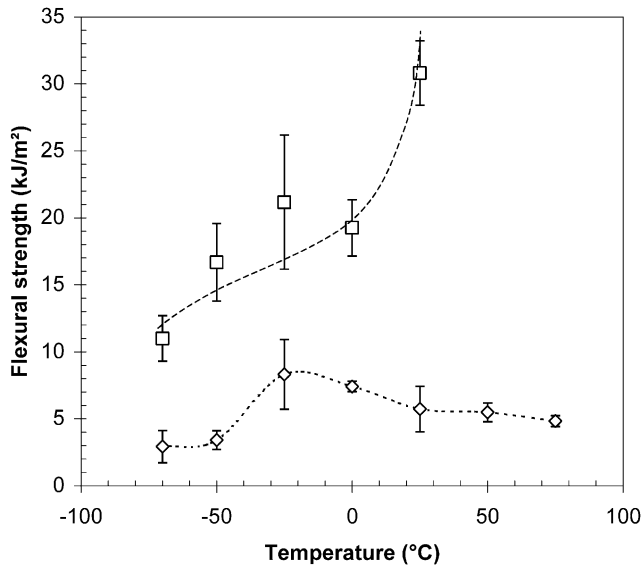
Fig. 7. Evolution of the flexural strength at break as a function of test temperature for D121/ST (□) and D121/DVB (◇).

(Fig. 7). As the temperature increases, the ability to plastic deformation is strongly enhanced for the D121/ST network with a factor around 5. A brittle-plastic transition can be clearly observed between 0 and 25 °C. In opposition, the flexural strength of D121/DVB network remains roughly constant with a low value with temperature. Even if elastic deformation is enhanced at high temperature because of a decrease in modulus, the very low deflection at break makes the flexural strength roughly constant.

3.2.3. Crack propagation analysis by AFM

For both networks, fracture surfaces after Charpy impact tests at 25 °C show a mirror-like surface which put into evidence a very fast crack propagation. AFM has been performed on such fractured surface in order to analyse crack propagation. For both networks, nodular surfaces, very similar to those observed after laser ablation, have been observed (Fig. 8). Those nodules are attributed to agglomerated microgels. It is well known [23] that the crack
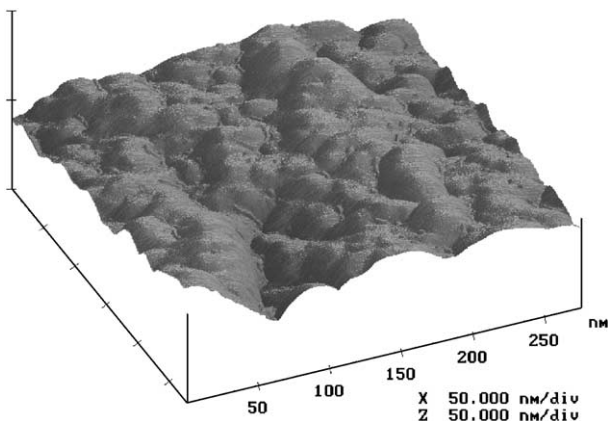

Fig. 8. Typical AFM observation of the fractured surfaces of networks after Charpy impact test.
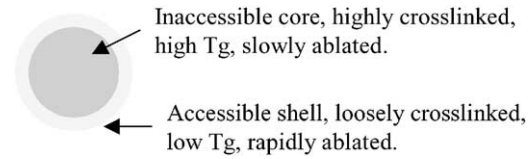

Fig. 9. Schematic representation of a microgel. Note that the boundaries are probably not sharp but a gradient of crosslink density.

propagates in the material via the points of weakness. Because a nodular surface is exhibited by the crack propagation, the weakest points in those networks should be located around microgels. No fractured microgels have been observed.

A single microgel could be drawn schematically in two parts as proposed in Fig. 9. The core of the microgel is defined as the inaccessible part of the particle. Reactive species located in this part are trapped and cannot participate to inter-microgel reactions because of steric hindrance and reduction of mobility due to crosslinking reactions. This inaccessible core is very densely crosslinked and as a consequence has a high T_g. This part of the microgel is also slowly ablated during laser treatment. By contrast, the outer shell of the microgel is loosely crosslinked and has a low T_g. The reactive species located in this shell can diffuse to react with other microgels to form clusters. This accessible shell is more rapidly ablated during laser treatment. Of course those two parts are not clearly separated and could not be defined as two phases. Those two parts scheme a gradient of crosslinking density and accessibility, in other words a continuous variation of properties between the shell and the core of a single microgel.

A tentative representation of the crack propagation in a network formed from microgels agglomeration is given in Fig. 10. We must not imagine sharp boundaries but rather boundaries showing a gradient of crosslinking density. Microgels are partially interpenetrated through their accessible shell. Black regions located at the intersection of several microgels consist of unreacted monomers to form some pools of monomers as proposed by Bowman [4]. A significant amount of voids has also been measured in those
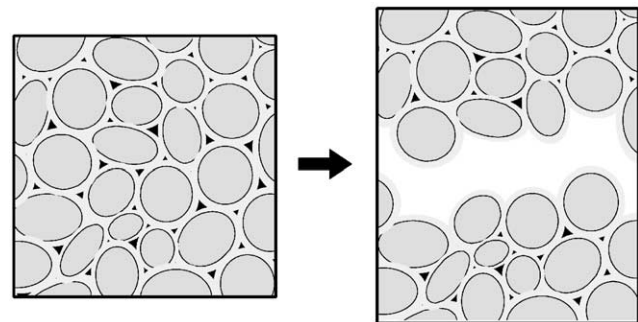

Fig. 10. Tentative schematic representation of crack propagation in a network formed by microgels agglomeration. Note that the boundaries are probably not sharp but a gradient of crosslink density.
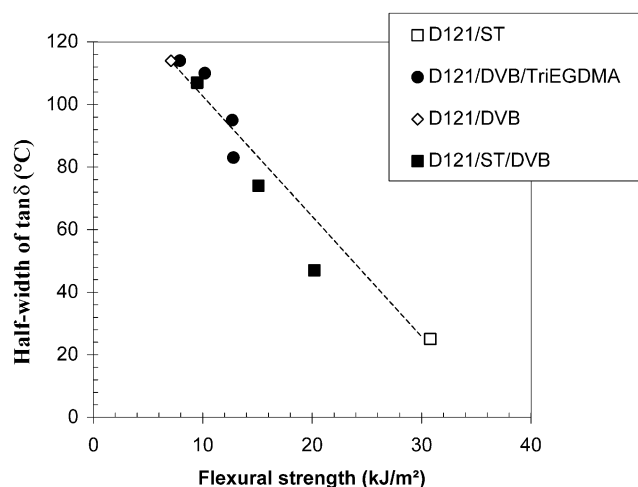
Fig. 11. Evolution of the half-width of tan δ as a function of the flexural strength for several networks synthesized from D121 with various comonomers.

networks in a previous study [24]. The average free volume fraction is 4.66% for the D121/ST network and 4.96% for the D121/DVB network. Those black regions can also be attributed to voids or region of very low crosslink density between microgels. The loosely crosslinked region formed by the shell of all microgels is probably continuous in the network and forms a weak region where a crack can propagate easily. This region can be compared to a weak loop in a chain. The very different structure between highly crosslinked regions and loosely crosslinked regions favours the appearance of defects.

The difference in average residual stresses measured between D121/ST and D121/DVB networks is also an important point to consider. These residual stresses after post-cure represent at 25 °C 9% of the maximum flexural stress for D121/ST and 22% for D121/DVB. First of all the average residual stresses can be considered as superimposed to the applied stress and second, this effect is magnified by the stress concentration effect due to the heterogeneous structure of the networks. If the fluctuation of crosslinking density is spatially organised around microgels in the network, a similar fluctuation must be considered for glass transition temperature. During material processing and especially during cooling from final post-cure temperature (120 °C) to room temperature, a fluctuation of residual stresses can appear. The highly crosslinked core of microgels will vitrify earlier than the loosely crosslinked shell of microgels. As a consequence, the fluctuation of residual stresses will be more important for the most heterogeneous network. The D121/DVB network has the most heterogeneous structure showing a broader distribution of relaxation times and crosslinking density, the highest level of residual stresses and probably the largest fluctuation of residual stresses. All those points could explain the higher brittleness of D121/DVB network compared to D121/ST one.

4. Conclusion

The brittleness of dimethacrylate-based networks is the consequence of the build-up of a structure by formation and agglomeration of microgels. The structural heterogeneity of such networks controls fracture behaviour. As plotted in Fig. 11 for various networks synthesized from D121 with various comonomers, the flexural strength decreases when the structural heterogeneity of the networks characterized by the half-width of tan δ increases. D121/DVB network is the most highly crosslinked network and exhibits the most heterogeneous structure, it has the lowest fracture resistance. In opposition, the D121/ST network has the lowest crosslinking density and its structure is more homogeneous, it has the best fracture resistance.

Acknowledgments

References

[1] Rey L, Galy J, Sautereau H, Lachenal G, Vial J, Henry D. Appl Spectrosc 2000;54(1):39.
[2] Rey L, Galy J, Sautereau H. Macromolecules 2000;33:6780.
[3] Dusek K. Angew Macromol Chem 1996;240:1.
[4] Bowman CN, Carver AL, Kennett SN, Williams MM, Peppas NA. Polymer 1990;31:135.
[5] Rey L. PhD INSA de Lyon; 2000. 270 p.
[6] Feng Y, Liu ZQ, Yi XS. Appl Surf Sci 2000;156:177.
[7] Benabdi M, Roche AA. J Adhes Sci Technol 1997;11:281.
[8] Mc Crum WG, Read BE, Williams G. Anelastic and dielectric effects in polymers. New York: Wiley; 1967.
[9] Allen PEM, Simon GP, Williams DRG, Williams EH. Macromolecules 1989;22:809.
[10] Kannurpatti AR, Anderson KJ, Anseth JW, Bowman CN. J Polym Sci, Part B: Polym Phys 1997;35:2297.
[11] Kannurpatti AR, Anseth JW, Bowman CN. Polymer 1998;39:2507.
[12] Young JS, Kannurpatti AR, Bowman CN. Macromol Chem Phys 1998;199:1043.
[13] Mortaigne B, Feltz B, Laurens P. J Appl Polym Sci 1997;66:1703.
[14] Bäuerle D, Himmelbauer M, Arenholz E. J Photochem Photobiol A: Chem 1997;106:27.
[15] Lazare S, Granier V. Laser Chem 1989;10:25.
[16] Costela A, Figuera JM, Florino F. Appl Phys 1995;60:261.
[17] Ziaee S, Palmese GR. J Polym Sci, Part B: Polym Phys 1999;37:725.
[18] Srivastava AK, White JR. J Appl Polym Sci 1984;29:2155.
[19] Shimbo M, Ochi M, Arai K. J Coat Technol 1984;56(713):45.
[20] Lange J, Manson JAE, Hult A. Polymer 1996;37(26):5859.
[21] Lange J, Toll S, Manson JAE, Hult A. Polymer 1997;38(4):809.
[22] Bogdal D, Pielikowski J, Boron A. J Appl Polym Sci 1997;66:2333.
[23] Simon G, Allen EM, Williams DG. Polym Engng Sci 1991;31(20):1483.
[24] Rey L, Galy J, Sautereau H, Simson GP, Cook WD. Submitted for publication.